J Fluoresc (2015) 25:1303–1314
DOI 10.1007/s10895-015-1618-x

ORIGINAL ARTICLE

Synthesis, Spectral Characteristics and DFT Studies of the New Dye 2,7-diacetyl-9-((dimethylamino)methylene)-9H-fluorene (DMMF) in Different Solvents

Abdullah M. Asiri[1] · Saleh A. Ahmed[3,4] · Samy A. El-Daly[1,2] · Mahmoud A. Hussein[1,3] · Amerah M. Al-Soliemy[1,5] · Osman I. Osman[1,5] · Mohamed R. Shaaban[4] · Ismail I. Althagafi[4]

Received: 5 April 2015 / Accepted: 5 July 2015 / Published online: 26 July 2015

Abstract The photophysical parameters such as electronic absorption spectra, molar absorptivity(ε), fluorescence spectra and fluorescence quantum yield (φ_f) of a new dye namely 2,7-diacetyl-9-((dimethylamino)methylene)-9H-fluorene (DMMF) were determined in different solvents. The electronic absorption are less sensitive to medium polarity. A bathochromic shift was observed in emission spectra(ca. 50 nm) upon increase of solvent polarity, which indicates that the singlet excited state (S_1) of DMMF is more polar than the singlet ground state (S_o). Solid crystals of DMMF exhibit intense yellow fluorescence maximum at 550 nm with bandwidth equal 64 nm upon excitation at wavelength 365 nm. The change in dipole moment value ($\Delta\mu$) was calculated by using the variation of Stokes shift with solvent polarizability (Δf) (Lippert – Mataga plot) and was found to be 7.22 and 5.5 Debye for higher and lower energy of $S_o - S_1$ (π-π^*) H-1→ *L* and $S_o - S_1$ (π-π^*) H→*L*, respectively. These results show that, the excited state is more polar than the ground state. The net photochemical quantum yields of photodecomposition of DMMF (φ_c) were calculated as 7.2×10^{-5}, 1.14×10^{-4}, 1.44×10^{-4} and 2.11×10^{-4} in different solvents such as MeOH, CH_2Cl_2, $CHCl_3$ and CCl_4, respectively. DFT/TD-DFT methods were used to study the geometric and electronic structures of DMMF in different solvents. A good agreement was found between the experimental and theoretical results.

Keywords 2,7-diacetyl-9-((dimethylamino)methylene)-9H--fluorene (DMMF) · Photophysical parameters · Fluorescence quantum yield · Photostability · DFT/TD-DFT studies

✉ Samy A. El-Daly
samyeldaly@yahoo.com

[1] Chemistry Department, Faculty of Science, King Abdulaziz University, PO Box 80203, Jeddah 21589, Saudi Arabia

[2] Chemistry Department, Faculty of Science, Tanta University, Tanta 2173, Egypt

[3] Chemistry Department, Faculty of Science, Assiut University, Assiut 71516, Egypt

[4] Chemistry Department, Faculty of Science, Umm Al-Qura University, Mecca, Saudi Arabia

[5] Chemistry Department, Faculty of Science, University of Khartoum, P.O.Box 321, Khartoum 11111, Sudan

Introduction

Nowadays, efficient fluorescent organic molecules have attracted widespread attention due to their sensible applications in sensors, displays, storage and photoelectronic devices [1–5]. The polycyclic aromatic hydrocarbons (PAH) have fulfill these applications and found to attract considerable attention, due to their intriguing molecular structures [1–3] and potential application in the emerging area of molecular electronics [4–7], including organic light-emitting diodes (OLEDs), organic field-effect transistors (OFETs) and organic photovoltaics (OPVs). Among the polycyclic aromatic hydrocarbons (PAH), fluorene molecule [8] which contains two benzene rings linked with a five-membered ring which provide a high overlaps of π-orbitals has been found to the most important fluorescent molecules and find the applications in polymers, electronic devices, sensors and photochromic materials as well [9–11].

Fluorene-based [12–15] materials have been extensively used as talented blue emitter for OLEDs. The fluorene groups are electron- rich aromatic units and have the ability play a role in enhancing the absorption properties and decreasing the

oxidation potential [16]. In addition the bulk and rigidity of the fluorene moiety is advantageous for civilizing the color purity and suppresses aggregation and excimer formation. Indeed, Fluorene shows interesting spectroscopic and photophysical properties. This fluorophore was extensively used as a building block for the development of dyes with good absorption properties [17] and fluorescence sensors [18]. In this work, new 2,7-disusituted fluorene, namely 2,7-diacetyl-9-((dimethylamino)-methylene)-9H-fluorene (DMMF) synthesized and its unique photophysical properties and density functional theory (DFT) has been used to optimize the geometry of the new dye to a minimum. In addition, the photo reactivity of DMMF dye in different solvents has been studied.

Experimental

Materials and Reagents

2,7-diacetyl-9H-fluorene (I) and dimethylformamide dimethylacetal (DMF-DMA) (II) and all solvents used were of spectroscopic grade and used without farther purifications. They were checked for the absence of absorbing or fluorescent impurities within the scanned spectral ranges.

Instrumentation

All melting points were measured on a Gallenkamp melting point apparatus. The infrared spectra were recorded in potassium bromide discs on FT-IR spectra were recorded on a Nicolet 6700 infrared spectrophotometers Thermo Fisher Scientific, with the KBr pellet technique. NMR was recorded on a Bruker AM 300 (1H: 300 MHz) and on Bruker Advance 600 MHz with $CDCl_3$ as solvents with tetramethylsilane (TMS) as the internal reference. Chemical shifts were related to that of the solvent. Mass spectra were recorded on a Shimadzu GCMS-QP1000 EX mass spectrometer at 70 eV. Elemental analyses were carried out at the Micro-analytical Centre of Cairo University, Giza, Egypt and recorded on Elementar-Vario EL automatic analyzer. UV–vis electronic absorption spectra was recorded on a Shimadzu UV-160A spectrophotometer, and the steady-state fluorescence spectra were measured using Shimadzu RF 5300 spectrofluorphotometer using a rectangular quartz cell of dimensions 0.2 cm × 1 cm. The emission was monitored at right angle. Light intensity of irradiation wavelength was measured using ferrioxalate actinometry [19]. The photochemical quantum yields (φ_c) of DMMF were measured using a modified method that takes into account the decrease in absorbance at the excitation wavelength as photo-irradiation proceeds [20].

The fluorescence quantum yield (φ_f) was measured using an optically diluted solution of quinine sulfate as reference standard according to Eq. (1) [21]:

$$\emptyset_f(s) = \emptyset_r \times \frac{\int I_s}{\int I_r} \times \frac{A_r}{A_s} \times \frac{n_s^2}{n_r^2} \quad (1)$$

where φ_r; φ_s are the fluorescence quantum yields of the unknown and standard, respectively, I is the integrated emission intensity; A is the absorbance at excitation wavelength, and n is the refractive index of the solvent.

Synthesis of 2,7-diacetyl-9-((dimethylamino)methylene) -9H-fluorene (DMMF)

2,7-diacetyl-9*H*-fluorene (**I**) (25 g, 100 mmole) was added to dimethylformamide-dimethylacetal *(DMF-DMA)*(II) (23.8 g, 200 mmol) and the mixture was refluxed for 15 min without solvent. The excess DMF-DMA was distilled off under reduced pressure and the residual reddish brown viscous liquid was taken in ethanol (20 ml) and the resulting orange crystal was collected by filtration, washed thoroughly with ether, dried and finally recrystallized from ethanol to afford the corresponding 2,7-diacetyl-(9-((dimethylamino)methylene)-9*H*-fluorene (DMMF) in (80 % yield), m.p 194 °C. The physical and spectral data of the synthesized compound are listed below:

Signal at δ 2.7 due to the methyl protons of the two acetyl groups, a singlet signal at δ 3.30 due to the methyl protons of *N,N*-dimethyl moiety, a singlet signal at δ 7.72 due to olefinic proton, in addition to an aromatic ring protons signals in the region δ 7.84–8.36.

IR (KBr) ν_{max}/cm^{-1}: 1672 (C=O), 1620 (C=N). ^{1}H NMR (DMSO-d_6): δ 2.71 (s, 6H, 2 (CH_3CO)), δ 3.38 (s, 6H, $N(CH_3)_2$), 7.72 (s, 1H, (CH=), 7.48–7.57 (m, 6H, ArH's), ^{13}C NMR (DMSO-d_6): δ 26.96, 27.01, 45.06, 105.17, 117.02, 120.22, 120.32, 122.58, 123.38, 123.68, 134.92, 135.24, 136.03, 137.22, 139.27, 142.36, 143.97, 198.51, 198.75; MS (m/z): 305 (M^+). Analysis for $C_{20}H_{19}NO_2$: Calcd: C, 78.66; H, 6.27; N, 4.59. Found: C, 78.62; H, 6.30; N, 4.55 %.

Results and Discussion

The versatile, hitherto unreported 2,7-diacetyl-9-((dimethylamino)-methylene)-9H-fluorene (DMMF) was readily obtained by refluxing 2,7-diacetyl-9H-fluorene (I) and dimethylformamide dimethylacetal (DMF-DMA) (II), without solvent shown in Scheme 1.

The structure of DMMF was confirmed by elemental and spectral analyses as described in the experimental part. For example, its ^{1}H-NMR spectrum displayed a singlet signal at

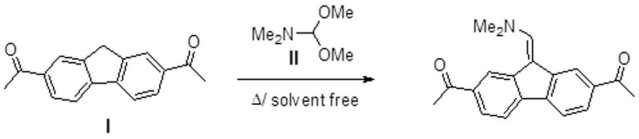

Scheme 1 Synthesis of 2,7-diacetyl-9-((dimethylamino)methylene)-9H-fluorene (DMMF)

δ 2.7 due to the methyl protons of the two acetyl groups, a singlet signal at δ 3.3 due to the methyl protons of N,N-dimethyl moiety, a singlet signal at δ 7.72 due to olefinic proton, in addition to an aromatic ring protons signals in the region δ 7.84–8.36.

Spectral Characteristics in Different Solvents

The electronic absorption, excitation and fluorescence spectra of (1×10^{-5} M) DMMF were measured in solvents of different polarity. Its absorption, excitation and emission spectra in several solvents are shown in Figs. 1, 2 and 3, and the corresponding spectral data are summarized in Table 1. As indicated in Figs. 1 and 2, DMMF shows an strong absorption band around 345 nm with high molar absorptivity (ε=27,800–38,900 mol dm^{-3} cm^{-1}) and a weak absorption band around 450 nm with low molar absorptivity (ε=6300–8900 mol dm^{-3} cm^{-1}). There is also a mirror image relationship between the absorption and fluorescence spectra and a coincidence between absorption and excitation maxima. These facts together with the higher molar absorptivities of the electronic transition of the dye are consistent with a strongly allowed transition $S_o - S_1$ (π-π*) with small geometry change between electronic ground and excited state of DMMF molecule. As shown in Table 1, the solvent polarity shows a slight effect on the position of electronic absorption and excitation spectral maxima (*ca.* 10 nm), indicating the less polar character of DMMF in the ground state. Also

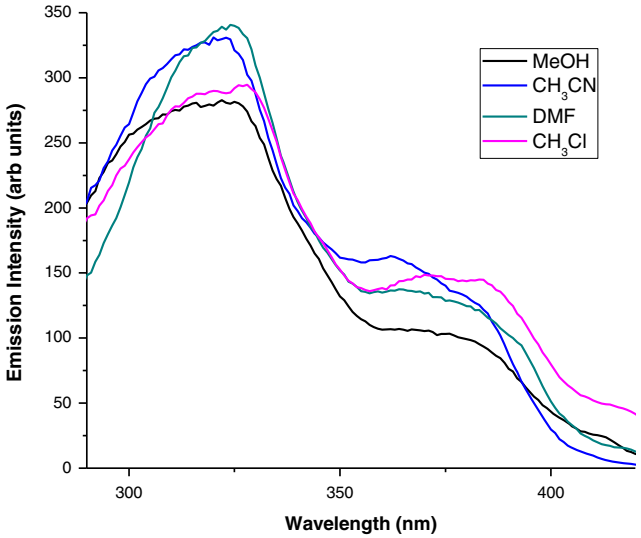

Fig. 2 Excitation spectra of 1×10^{-5} M DMMF in selected solvents (At $\lambda_{em.\ max.}$)

fluorescence spectra of DMMF show an intense emission band around 460 nm and a relatively weak emission band in the higher wavelength side corresponding to two transitions of S_1-S_o (π- π*). As shown in Fig. 3 and Table 1, the fluorescence spectra of DMMF are more sensitive to solvent polarity. As the solvent polarity increases, the emission spectra become red-shifted (*ca.* 50 nm). This indicates that the singlet excited state of the DMMF is more polar than the ground state due to electron transfer from amino group (electron donor) to keto-acetyl groups (electron acceptor) upon excitation.

Solid crystals of DMMF exhibit intense yellow fluorescence maximum at 550 nm with bandwidth equal 64 nm upon excitation at wavelength 365 nm (Fig. 4). With the change in the excitation wavelength from 365 to 450 nm, the position of the emission remains unchanged, which suggests that this

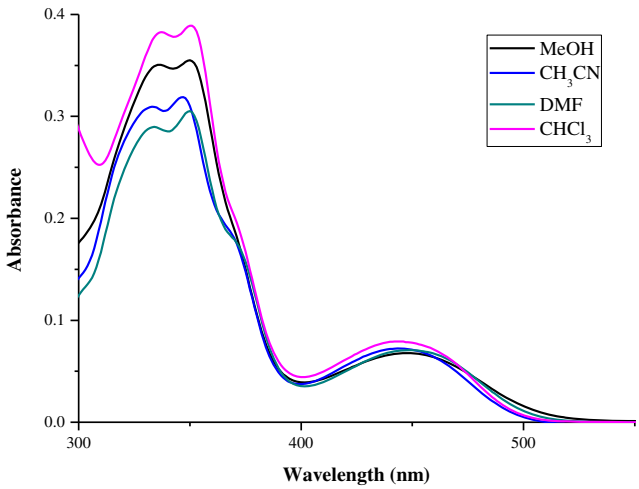

Fig. 1 Electronic absorption spectra of 1×10^{-5} M DMMF in selected solvents

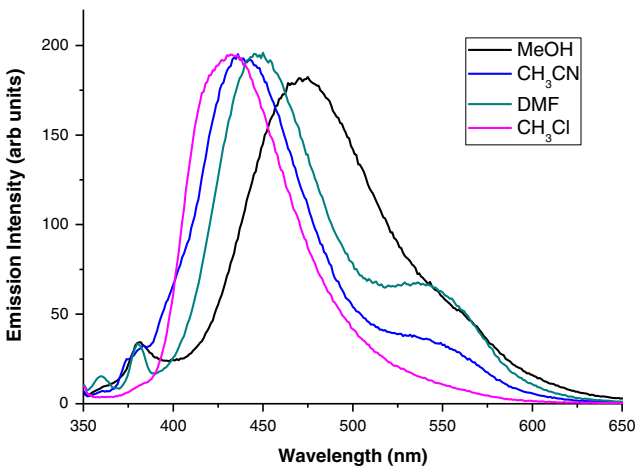

Fig. 3 Emission spectra of 1×10^{-5} M DMMF in selected solvents. ($\lambda_{ex.}$=340 nm)

Table 1 Spectral data for DMMF in different solvents

Solvents	$\Delta f(D,n)$	λ_{abs} (nm) $S_0 \rightarrow S_1$		λ_{em} (nm) $S_1 \rightarrow S_0$		$\Delta\bar{\nu}$ (cm^{-1})		ε M^{-1} cm^{-1} at		ϕf
		$\lambda_{(max\ 1)}$	$\lambda_{(max2)}$	$\lambda_{(max1)}$	$\lambda_{(max2)}$	$\Delta\bar{\nu}$ (1)	$\Delta\bar{\nu}$ (2)	$\lambda_{abs\ (max\ 1)}$	$\lambda_{abs\ (max\ 2)}$	
THF	0.210	346	437	429	508	5591	3103	27,800	6700	0.022
Dioxane	0.021	347	440	430	527	5563	3752	35,600	8400	0.036
Acetonitrile	0.304	347	443	432	536	5670	3917	31,900	6900	0.048
DMSO	0.263	352	452	454	591	6383	3878	34,300	8100	0.047
DMF	0.274	350	448	447	541	6200	3837	30,500	7000	0.042
CCl_4	0.115	335	430	394	522	4470	4025	36,800	8900	0.064
Chloroform	0.148	351	442	426	509	5016	2978	38,900	8240	0.042
CH_2Cl_2	0.218	349	443	420	513	4844	3080	36,400	8100	0.036
Methanol	0.308	350	444	473	562	7430	4729	35,500	6300	0.036
Ethanol	0.288	349	444	459	559	6867	4633	34,100	6300	0.043
Butanol	0.263	350	444	459	560	6785	4855	36,800	6300	0.054
Eg	0.300	353	457	497	566	7452	4214	35,100	6800	–

$\Delta\bar{\nu}$ (1) = $\lambda_{abs\ (max\ 1)}$ - $\lambda_{em\ (max\ 1)}$

$\Delta\bar{\nu}$ (2) = $\lambda_{abs\ (max\ 2)}$ - $\lambda_{em\ (max\ 2)}$

band is a true emission band and not due to any second order diffraction of the excitation light [22–24] (Fig. 5).

Such behaviour was attributed to emission from exciton state whose fluorescence is 100 and 60 nm red shifted compared to emission from 1×10^{-5} to 1×10^{-3} mol dm^{-3} in chloroform, respectively. This indicates that the crystal structure of DMMF belongs to β-type classification [25]. Solid-state photo luminescent substances are very interesting for several high-technology applications such as the fabrication of light emitting diodes [26]. No significant changes in emission intensity of DMMF crystalline solids upon prolonged irradiation with 365 and 450 nm for 180 min were observed. This fact leads to the high photo stability of DMMF in the solid state as shown in Fig. 6.

Estimation of Dipole Moments Using Solvatochromic Methods

Analysis of the solvatochromic effect allows the estimation of the difference in dipole moments ($\Delta\mu=\mu_e-\mu_g$) between the excited singlet and the ground state for two electronic absorption peaks in $S_o - S_1$ (π-π^*) (H-1→*L* and H→*L*) and

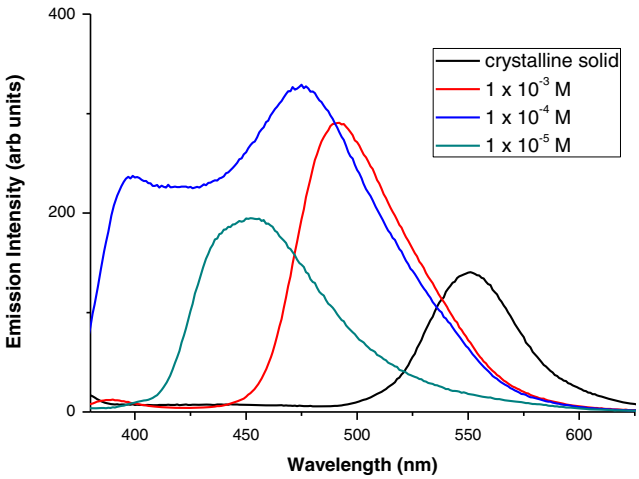

Fig. 4 Emission spectra of different concentrations of DMMF in CH_3Cl and in crystalline solid . ($\lambda_{ex.}$=340 nm)

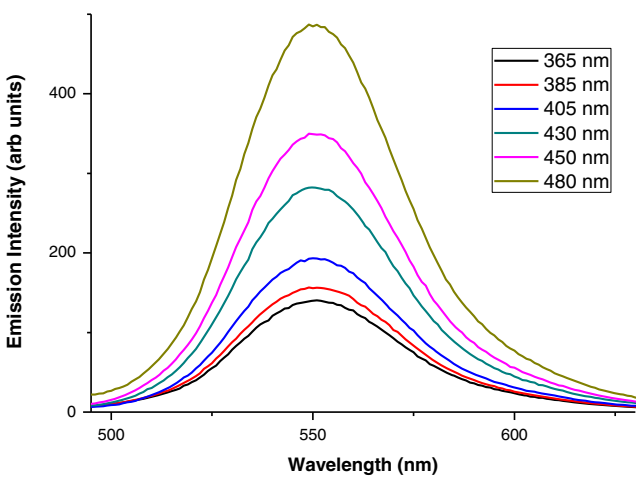

Fig. 5 Emission spectra of crystalline solid of DMMF at different excitation wavelengths

corresponding emission bands. This was achieved by applying the simplified Lippert – Mataga Eq. (2) [27, 28].

$$v_a - v_f = \frac{2\left(\mu_e - \mu_g\right)^2}{hca^3}\Delta f + constant \quad (2)$$

$$\text{where} \quad \Delta f(\varepsilon, n) = \left[\frac{(\varepsilon - 1)}{(2\varepsilon + 1)}\right] - \left[\frac{(n^2 - 1)}{(2n^2 + 1)}\right] \quad (3)$$

where $\Delta\overline{\nu}_{st}$ is the Stokes shift which increases with increasing in solvent polarity pointing to stronger stabilization of the excited state in polar solvents, h is Planck's constant, c is the speed of light in vacuum, a is the Onsager cavity radius, ε and n are the dielectric constant and refractive index of the solvent, respectively, μ_e and μ_g are the dipole moments of the excited and ground state, respectively. The Onsager cavity radius was taken as 4.2Å, which is comparable to the radius of a typical aromatic fluorophore [29].Figures 7 and 8 show the plot of Stokes shift versus the orientation polarization (Δf). The data in polar protic solvents were excluded to avoid specific solute-solvent interactions (hydrogen bonding). The change of dipole moments of DMMF upon excitation were calculated from the slope of the plot and the cavity radius as 7.22 and 5.5 Debye for higher and lower energy of $S_o - S_1$ (π-π^*) H-1$\rightarrow L$ and $S_o - S_1$ (π-π^*) H$\rightarrow L$, respectively. This change in dipole moment is caused by redistribution of atomic charges in the excited state because of charge transfer from the electron-rich amino group to the electron acceptor keto-acetyl groups.

Photo Reactivity of DMMF Dye

The photo reactivity of DMMF has been studied in different solvents namely MeOH, CH_2Cl_2, $CHCl_3$ and CCl_4. Upon irradiation of 1×10^{-5} mol dm^{-3} of DMMF at 365 nm (I_o=4.5×10^{-4} Einstein min^{-1}), the absorbance of DMMF decreased with increasing the irradiation time until a photo stationary state was reached. As shown in Figs. 9, 10, 11 and 12, no new absorption appeared indicating the absence of photoproduct. The net photochemical quantum yields of photodecomposition of DMMF (φ_c) were calculated as 7.2×10^{-5}, 1.14×10^{-4}, 1.44×10^{-4} and 2.11×10^{-4} in MeOH, CH_2Cl_2, $CHCl_3$ and CCl_4, respectively. These results indicate that DMMF is more stable in MeOH than in any of the chlorinated solvents. It seems that the photodecomposition of DMMF in chloromethane solvents takes place by electron transfer from the excited DMMF molecule to the solvent according to a well-known mechanism [30–37].

It was proposed that the electron transfer from the excited singlet DMMF to CH_nCl_{4-n} within transient excited charge transfer complex (exciplex) is the main primary photochemical process. It leads to DMMF radical cation, a chloride ion and a chloromethyl radical in solvent cage. The formation of contact ion pair usually occurs by electron transfer from

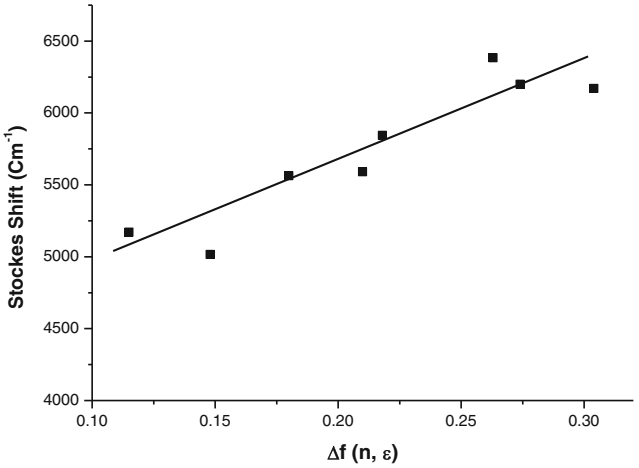

Fig. 7 Plot of Stockes Shift versus Δ_f value

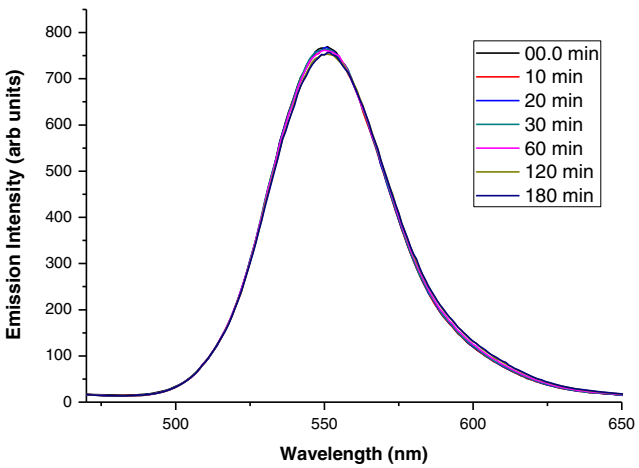

Fig. 6 Effect of radiation on the emission spectrum of crystalline solid DMMF ($\lambda_{irr.}$=430 nm)

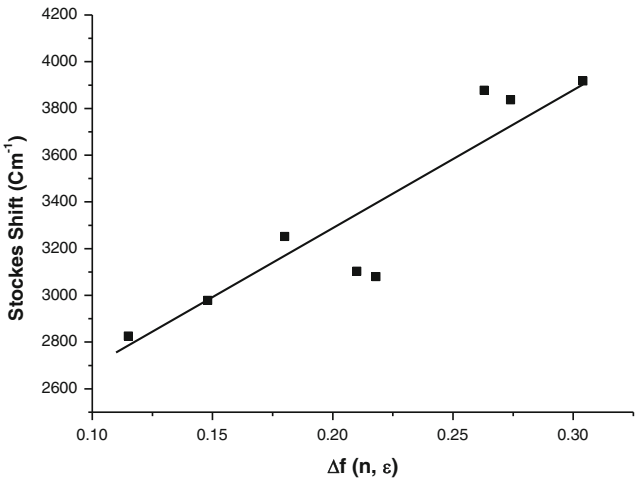

Fig. 8 Plot of Stockes Shift versus Δ_f value

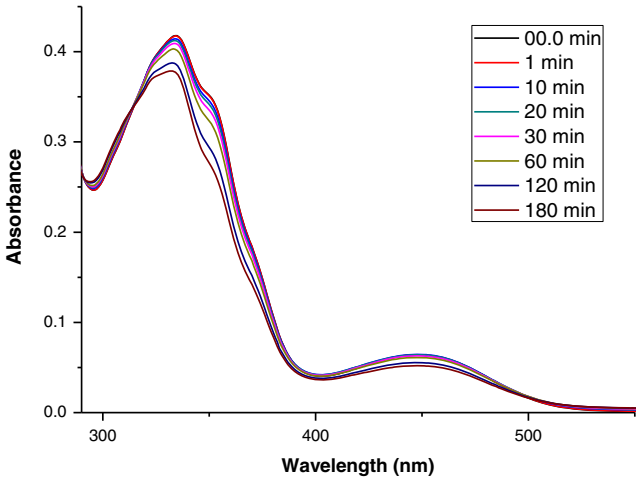

Fig. 9 Effect of radiation on the absorption spectrum of 1×10^{-5} M DMMF in MeOH ($\lambda_{irr.}$=365 nm)

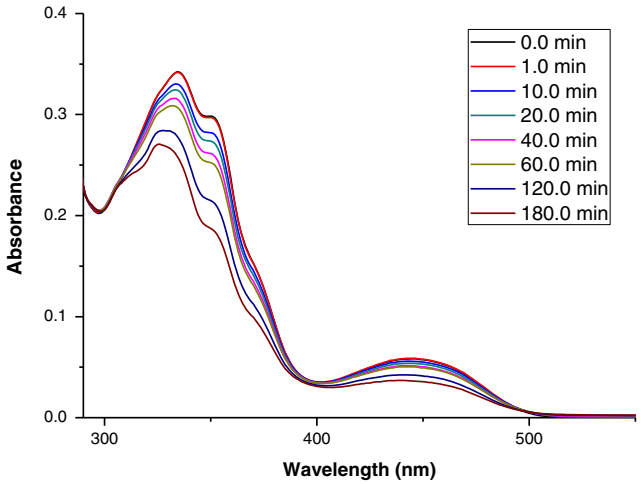

Fig. 11 Effect of radiation on the absorption spectrum of 1×10^{-5} M DMMF in $CHCl_3$ ($\lambda_{irr.}$=365 nm)

excited donor to the electron acceptor depending on the electron affinity (E_A) of acceptor.

$$(\mathrm{DMMF}) + h\nu \rightarrow {}^1(\mathrm{DMMF})^* \quad \text{absorption of light} \tag{4}$$

$${}^1(\mathrm{DMMF})^* \rightarrow \mathrm{DMMF} + h\nu \quad \text{fluorescence} \tag{5}$$

$${}^1(\mathrm{DMMF})^* + \mathrm{CH_nCl_{4-n}} \rightarrow {}^1[\mathrm{DMMF}\ldots\mathrm{CH_nCl_{4-n}}]^* \quad \text{exciplex} \tag{6}$$

$${}^1[\mathrm{DMMF}\ldots\mathrm{CH_nCl_{4-n}}]^* \rightarrow [\mathrm{DMMF}^{+\delta}\ldots{}^{-\delta}\mathrm{CH_nCl_{4-n}}] \quad \text{electron transfer} \tag{7}$$

$$[\mathrm{DMMF}^{+\delta}\ldots{}^{-\delta}\mathrm{CH_nCl_{4-n}}] \rightarrow \mathrm{DMMF}^{\cdot+\delta}\mathrm{Cl}^- + {}^{\cdot}\mathrm{CH_nCl_{3-n}} \quad \text{contact ion pair} \tag{8}$$

DFT Calculation

The ab initio molecular orbital calculations were performed using the Gaussian09 package of programs [38] and visualized by the Gauss Veiw software [39]. The hybrid Becke's three parameter Lee-Young-Parr correlation functional (B3LYP) with double-zeta and polarization functions on heavy atoms basis set [6-31G(d)] of the density functional theory (DFT) has been used to optimize the geometry of the New Dye to a minimum. The harmonic vibrational frequencies were analytically evaluated by obtaining the second derivatives of the energy using the same level of theory. The ^{1}H and ^{13}C NMR chemical shifts relative to TMS within the GIAO approach [40] were computed by using HF/6-31G(d) level of theory at B3LYP/6-31G(d) optimized geometry. The UV–vis. spectra of the New Dye in Tetrahydrofuran (THF), methanol (MeOH), dichloromethane (CH_2Cl_2) chloroform

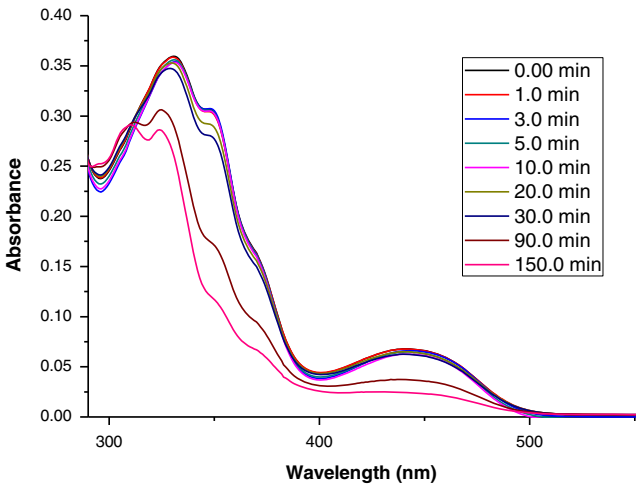

Fig. 10 Effect of radiation on the absorption spectrum of 1×10^{-5} M DMMF in CH_2Cl_2 ($\lambda_{irr.}$=365 nm)

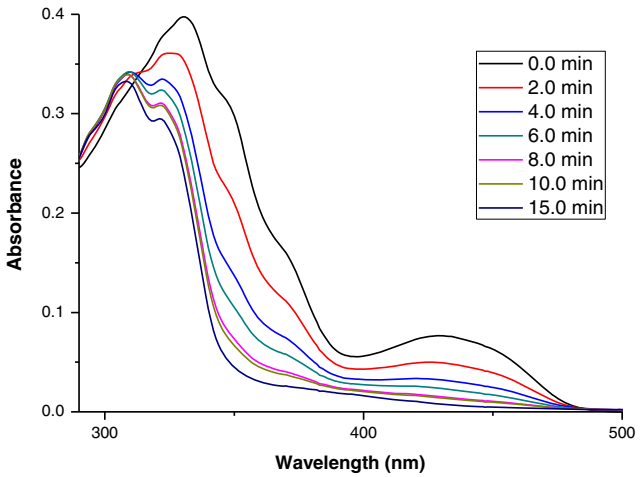

Fig. 12 Effect of radiation on the absorption spectrum of 1×10^{-5} M DMMF in CCl_4 ($\lambda_{irr.}$=365 nm)

Table 2 Some selected bond lengths (Å) and bond angles (degrees) for gas phase DMMF which have been calculated at B3LYP/631G(d) level of theory

Designation	Bond length (Å)	Designation	Bond angle (degree)
N22-C20	1.347	C27-N22-C20	120.09
C20-C19	1.382	C20-N22-C23	124.44
C19-C4	1.467	N22-C20-C19	132.23
C4-C3	1.398	C20-C19-C10	120.25
C3-C2	1.403	C10-C11-C12	120.06
C2-C37	1.494	C12-C13-O36	120.90
C37-O42	1.229	C11-C10-C19-C4	179.79
C37-C38	1.518	C10-C19-C4-C3	171.30
C4-C5	1.433	C4-C19-C20-N22	20.17
C5-C6	1.400	C19-C20-N22-C27	−168.16
C5-C15	1.450	C19-C20-N22-C23	18.37

($CHCl_3$) and carbon tetrachloride (CCl_4) solvents were estimated by using Time-Dependent density functional theory (TD-DTF) [41] and the polarizable continuum model (PCM) method [42] with the B3LYP/631G(d) model chemistry.

Geometry

Table 2 lists some of the bond lengths and angles of the optimized geometry of the title molecule (Fig. 13) which have been computed by using B3LYP/631G(d) level of theory. A number of remarks can be extracted from Table 2 and Fig. 13: (1) The environment around the amine moiety is almost flat and not pyramidal as expected. A partially multiply bonded N22-C20 bond facilitates this situation. It has a bond length of 1.347 Å, which is *ca.* 0.12 Å shorter than the C-N single bond on trimethylamine [43]. (2) The dimethyl methylene amine group makes a dihedral angle of *ca.* 31° with the fluorene moiety. (3) The fluorene motif itself is not exactly flat with a deviation of 1.8° between the planes of the pentagonal and benzene rings. (4) The two benzene rings are almost co-planar with the acetate groups on each side. Our results are in complete agreement with that of Gerkin et al. [44]. Consequently, this optimized geometry was adopted for studying its electronic and spectral properties in gas-phase and some selected solvents.

FTIR Vibrational Spectra

Our work involves satisfactory assignments of the vibrational modes of the title molecule using FTIR spectroscopy with a help of theoretical predictions. All the vibrational frequency calculations were computed after optimizing the geometry of DMMF to its minimum (no imaginary frequencies). Table 3 lists the observed anharmonic vibrational frequencies, which were recorded for DMMF in KBr discs, together with the corresponding harmonic gas-phase theoretical ones. The computed frequencies were obtained by using B3YP/6-31G level of theory and scaled [45] by a factor of 0.991. It is apparent that there is an overall good agreement between the observed and calculated values. Nonetheless, the latter vibrational modes are slightly higher than the former counterparts are. These discrepancies are attributed to some factors that include

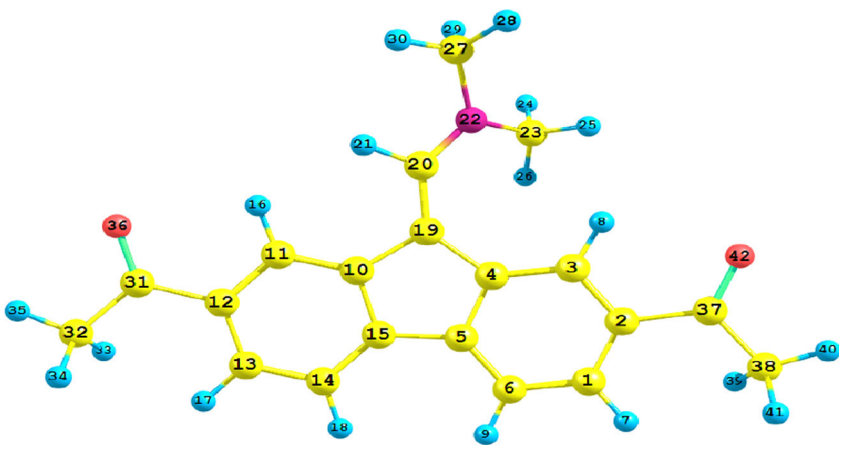

Fig. 13 The optimized geometry of DMMF in the gas-phase showing the atom numbering which has been obtained by using B3LYP/631G(d) level of theory

Table 3 The observed (KBr discs) and calculated vibrational wavenumbers (cm^{-1}) for DMMF in the gas-phase. The scaled (0.991)[a] calculated values were obtained by using B3LYP/6-31G(d) level of theory

Assignment	Experimental	Theoretical
υ aromatic C-H str.	3065–3110	3164–3233
υ aliphatic C-H str.	2910–2980	3019–3162
υ C=O sym. stretch	1672	1726
υ C=O asym. stretch	1672	1723
υ C=N str.	1620	1655
υ aromatic C=C str.	1585–1650	1593–1631
υ CH_3 bend	1498	1500–1538
υ CCH aromatic bend	1492	1486–1496
υ C-C stretch.	1295	1367

[a] Computational Thermochemistry: Scale Factor Databases and Scale Factors for Vibrational Frequencies Obtained from Electronic Model Chemistries,"I. M. Alecu, J. Zheng, Y. Zhao, and D. G. Truhlar, *J. Chem. Theory Comput.* **6**, 2872–2887 (2010)"

mainly the electron correlation effect, insufficient basis set and the difference in mode and phase i.e., the experimental frequencies are anharmonic and recorded in the solid phase while their theoretical rivals are harmonic and estimated in the gas-phase. Briefly, both the experimental and theoretical vibrational modes are in conformity with the predicted geometry.

Table 4 The observed and calculated ^{1}H and ^{13}C chemical shifts (ppm) (with respect to TMS) for DMMF. The calculated values were obtained by using HF/6-31G/B3LYP/6-31G(d) level of theory

Atom	Theoretical	Experimental
C38	36.528	26.96
C32	36.588	27.01
C23	51.789	45.06
C27	55.272	45.45
C19	111.953	105.17
C11	122.288	117.02
C14	124.305	120.22
C6	124.436	120.32
C3	127.709	122.58
C13	128.427	123.38
C1	128.705	123.68
C2	136.757	134.92
C12	137.548	135.24
C4	141.560	136.03
C15	141.885	137.22
C5	144.062	139.27
C20	145.472	142.36
C10	147.687	143.97
C31	198.002	198.51
C37	198.165	198.75
4H(CH3O)	2.309–3.020	2.71
6H(CH3N)	3.333–4.195	3.38
7H(ArH)	7.635–8.981	7.48–7.57

NMR Chemical Shifts

In Table 4 are listed the calculated GIAO ^{1}H and ^{13}C NMR shifts using HF/6-31G/B3LYP/6-31G level of theory together with the experimental chemical shifts with respect to TMS values for the title compound . The estimated aromatic C-H ^{1}H chemical shifts with respect to TMS showed up between 7.635 and 8.981 ppm, whereas their observed rivals appeared between 7.48 and 7.57 ppm. The experimental ^{1}H NMR values for CH_3N moieties arouse around 3.38 ppm compared to their theoretical counterparts that lied around 3.333–4.195 ppm. The experimental ^{1}H signals for the CH_3O hydrogens showed up around 2.71 ppm but arose theoretically at 2.309–3.020 ppm. The measured two $^{13}CH_3CO$ NMR signals showed up between 26.96 and 27.01 ppm; while their calculated rivals lied around 36.528–36.588 ppm. The experimental signals for the two $^{13}CH_3N$ atoms are found around 51.789–55.272 ppm; while their theoretical counterparts occur around 45.06–45.45 ppm. The experimental fluorene group ^{13}C NMR chemical shifts showed up between 105.17 and 198.75 ppm, whereas their estimated rivals showed up around 111.953–198.165 ppm. It is evident that the computed ^{1}H and ^{13}C NMR chemical shifts for the title compound are in excellent agreement with their experimentally observed values. These NMR experimental and theoretical structure elucidations of DMMF are in line with its optimized geometry listed in Table 2.

UV-Visible Spectra

$\pi\rightarrow\pi^*$ and $n\rightarrow\pi^*$ transitions are thought to be responsible for UV-visible absorption spectra of π-conjugated organic molecules [46]. These transitions embrace electron motions between frontier orbitals, especially between the higher occupied molecular orbitals (HOMOs) and the lower unoccupied molecular orbitals (LUMOs). The title compound DMMF has many double bonds together with lone pairs in the oxygen and nitrogen atoms. The experimental and theoretical UV-Visible excitations of DMMF in CH_3OH, CH_2Cl_2, $CHCl_3$ and CCl_4 are shown in Figs. 9, 10, 11 and 12. Table 5 lists their nature and assignments aided by calculations using PCM method at TD-B3LYP/6-31G level of theory in the same solvents. The observed UV-Visible bands for DMMF in the chosen solvents showed up at 335–350, 369–370 and 430–444 nm, while their corresponding theoretical transitions are computed around 352–360, 361–373 and 508–540 nm, respectively. There is good agreement between the experimental and theoretical peaks in trend. The differences in magnitudes were larger for H→L, followed by H-1→L and least for H→L+1. The

Table 5 The UV–vis. observed and calculated wavelengths (λ/nm) for DMMF in different solvents. Their transition energies (eV), oscillator strengths and assignments were facilitated by using TD-B3LYP/6-31G(d) level of theory

Solvent	Wavelength λ/nm		Energy/eV	Oscillator strength	Assignment
	Experimental	Theoretical			
MeOH	350	360.22	2.295	0.115	H-1→L
	370 sh	373.88	3.316	0.001	H→L+1
	444	540.32	3.304	0.780	H→L
CH_2Cl_2	349	356.54	3.477	1.059	H-1→L
	370 sh	370.94	3.342	0.0029	H→L+1
	443	532.32	2.329	0.1037	H→L
$CHCl_3$	351	352.67	3.516	0.9319	H-1→L
	369 sh	367.70	3.372	0.0066	H→L+1
	442	523.82	2.367	0.0927	H→L
CCl_4	335	353.55	3.507	0.0008	H-1→L
	370 sh	361.35	3.431	0.0158	H→L+1
	430	508.00	2.440	0.0745	H→L

maximum absorption peaks were predicted at 540.32, 532.32, 523.82 and 508.00 nm in MeOH, CH_2Cl_2, $CHCl_3$ and CCl_4 respectively; while these transitions were observed at 444, 443, 442 and 430 nm, respectively. These discrepancies can be attributed to the solvent effects i.e., the solvents make the chemical environments of the molecule become very complicated [47] and, to a lesser extent, perhaps to the insufficient basis set and inappropriate functional used. This point will be discussed further in the next section.

Frontier Orbitals

Figure 14 depicts the frontier orbitals of the title molecule DMMF in the gas-phase. They have been computed by using B3LYP/6-31G(d) level of theory. On the one hand, the HOMO is localized mainly on C19-C20 moiety and the nitrogen atom as π-bonding and lone pair, respectively; while the one beneath it (HOMO-1) is centered on the fluorene group as π-bonding orbitals

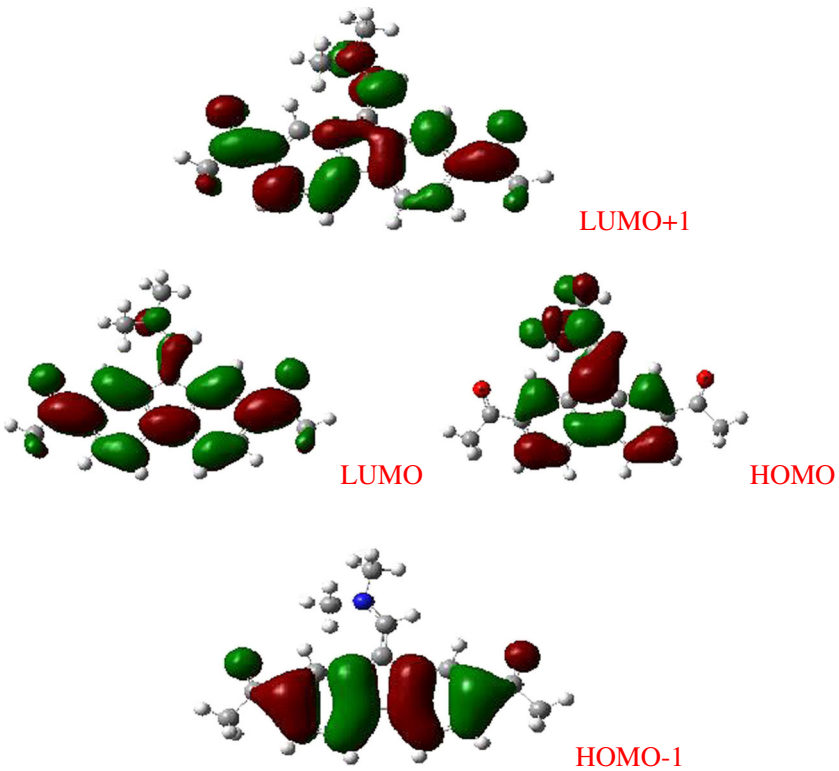

Fig. 14 The frontier orbitals of the gas-phase DMMF which have been calculated by using B3LYP/631G(d) level of theory

Table 6 The ground state total electronic energy (au), relative energy (ΔE/kcal/mol), the dipole moment (D.M./Debye), the HOMO (eV), LUMO (eV) the energy gap (E.G./eV), the electronic chemical potential (μ/eV), the chemical hardness (η/eV) and the global electrophilicity index (ω/eV) for DMMF in different solvents. They been calculated using B3LYP/631G(d) level of theory

Parameter	Gas-phase	MeOH	CH_2Cl_2	$CHCl_3$	CCl_4
Energy	−978.7966	−978.7903	−978.7885	−978.7864	−978.7824
ΔE	0.000	3.938	5.117	6.403	8.898
D.M.	1.556	1.840	1.760	1.670	1.499
HOMO	−5.140	−5.005	−4.999	−4.995	−4.995
LUMO	−2.000	−2.168	−2.136	−2.104	−2.047
E.G.	3.140	2.837	2.863	2.891	2.948
μ	3.570	3.587	3.568	3.550	3.521
η	1.570	1.419	1.432	1.446	1.474
ω	4.059	4.534	4.445	4.358	4.205

and on the two oxygen atoms in the form of lone pairs. On the other hand, the LUMO is distributed all over the fluorene moiety as π*-antibonding orbital; whereas that above it is delocalized over the entire dye as π*-antibonding orbital.

Table 6 lists the total energies, the dipole moments and energies of the HOMOs and LUMOs together with their energy gaps (E.G.) of the gas-phase and the solvated DMMF substrates. The relative total energies of DMMF solvated substrates with respect to the gas-phase compound were also included. It is clear that the gas-phase compound is more stable than any of the solvated DMMF substrates by not less than 3.9 kcal/mol. In terms of the total electronic energy, the order of the stability of DMMF in the elected solvents is: MeOH > CH_2Cl_2 > $CHCl_3$ > CCl_4. This trend is in line the magnitudes of the ground state dipole moments of the solvated DMMF substrates as signs of non-uniform distribution of charges on the various atoms of the molecule.

The energy gaps (E.G.) of the gas-phase and the solvated DMMF substrates listed in Table 6, can be used as gauges for the intramolecular and intermolecular charge transfer within DMMF and between DMMF and the different solvents, respectively. It is clear that the energy gaps of 2.837–3.140 eV facilitate the π→π*, n→π* and n→σ* charge transfer as shown experimentally by the UV-Visible spectra. It is noteworthy that the energy gaps of the solvated DMMF substrates are less than that of its gas-phase form. This fact facilitates the intermolecular charge transfer between DMMF and the elected solvents. The order of decrease in the energy gaps of the solvated DMMF substrates is: MeOH > CH_2Cl_2 > $CHCl_3$ > CCl_4 which is line with the polarities of these solvents.

The maximum absorption peaks (λ_{max}) are due mainly to transitions between the HOMOs and LUMOs [47]. From DFT calculations, these intense transitions were evaluated for DMMF, using the relation: $\lambda_{max} = hc/\Delta E_{HOMO\text{-}LUMO}$, as 437, 433, 429 and 421 nm in MeOH, CH_2Cl_2, $CHCl_3$ and CCl_4 respectively. They are extremely close to their experimental (444, 443, 442 and 430 nm, respectively) rivals in both magnitude and trend.

Table 6 depicts also the electronic chemical potential (μ) that dictates the escaping tendency of electrons in a chemical system [48], the chemical hardness (η) as a helpful notion for investigating stability and reactivity of chemical systems [49] and the global electrophilicity index (ω) that estimates the stabilizing energy when a chemical species accepts additional electronic charge from the environment [48]. The η and μ values indicate that DMMF in MeOH is the softest, least stable and most reactive among them, while that in CCl_4 being the harder, most stable and least reactive. Furthermore, the ω values denote that DMMF in MeOH is a strongest electrophile amongst the solvated DMMF substrates, but it turns out to be the weakest electrophile (or a nucleophile) when dissolved in CCl_4 [50].

Table 7 Some selected second order perturbation ($E_{(2)}$) estimation of the hyperconjugative energies (kcal/mol) of the title molecule DMMF which were calculated using B3LYP/631G(d) level of theory

Interaction	Energy	Interaction	Energy
$\pi_{C2\text{-}C3} \rightarrow \pi^*_{C37\text{-}O42}$	19.85	$n_{N22} \rightarrow \pi^*_{C19\text{-}C20}$	50.84
$\pi_{C4\text{-}C5} \rightarrow \pi^*_{C2\text{-}C3}$	22.88	$n_{O36} \rightarrow \sigma^*_{C19\text{-}C20}$	18.76
$\pi_{C10\text{-}C15} \rightarrow \pi^*_{C4\text{-}C5}$	19.34	$n_{O36} \rightarrow \sigma^*_{C31\text{-}C32}$	19.63
$\pi_{C10\text{-}C15} \rightarrow \pi^*_{C11\text{-}C12}$	22.88	$n_{O42} \rightarrow \sigma^*_{C2\text{-}C37}$	18.68
$\pi_{C11\text{-}C12} \rightarrow \pi^*_{C13\text{-}C14}$	19.40	$n_{O42} \rightarrow \sigma^*_{C37\text{-}C38}$	19.62

Natural Bond Orbital Analysis

It has become widely known that the Natural Bond Orbital (NBO) theory [51, 52] is quite rewarding in analyzing hyperconjugative interactions [53]. This is done through applying second order perturbation energies ($E_{(2)}$):

$$E_{(2)} = \Delta E_{ij} = q_i \left(F_{ij}\right)^2 / \Delta\varepsilon$$

Where q_i is the donor orbital occupancy, F_{ij} is the off-diagonal elements of the NBO Kohn-Sham Matrix and $\Delta\varepsilon$ is the energy difference between a donor orbital (i) and an acceptor orbital (j). In Table 7 are listed the most influential second order perturbation ($E_{(2)}$) delocalization energies of DMMF in the gas-phase. These energies were estimated by using B3LYP/6-31G(d) level of theory. They are classified as $\pi\rightarrow\pi^*$, $n\rightarrow\pi^*$ and $n\rightarrow\sigma^*$ interactions. The strongest delocalization in DMMF involves the interaction of the nitrogen atom lone pair with the C19-C20 π-antibond ($n_{N22}\rightarrow\pi^*_{C19\text{-}C20}$). This interaction contributed 50.84 kcal/mol to the stabilization of DMMF. The most stabilizing $\pi\rightarrow\pi^*$ interactions are the C4-C5 and C10-C15 π-bonds with their synperiplanar C3-C2 and C11-C12 π-antibonds. These $\pi C4_{\text{-}C5} \rightarrow\pi^*_{C2\text{-}C3}$ and $\pi C10_{\text{-}C15} \rightarrow\pi^*_{C11\text{-}C12}$ delocalizations stabilized DMMF by 21.88 kcal/mol each. All these delocalizations are indicative of the intramolecular charge transfer from the $(CH_3)_2N$ moiety toward the two CH_3CO groups and through the fluorene motif. These findings are in excellent agreement with our experimental UV-Visible spectra.

Conclusion

In summary, we have synthesized a new pi-conjugated electron donor – acceptor type fluorene derivative DMMF having intramolecular charge transfer characteristics. The structure of this dye was identified by spectroscopic techniques. A red shift in emission spectrum of DMMF was observed upon increasing the solvent polarity, due to intramolecular charge transfer and intermolecular hydrogen between solute and solvent. Dipole moment calculation results suggest that the excited state of DMMF is more polar than the ground state. The pronounced change in dipole moment value ($\Delta\mu$) was calculated by using the variation of Stokes shift with solvent polarizability (Δf) (Lippert – Mataga plot) and was found to be 7.22 and 5.5 Debye for higher and lower energy of $S_o - S_1$ (π-π^*) H-1→ *L* and $S_o - S_1$ (π-π^*) H→ *L*, respectively. These results proved that, the excited state is more polar than the ground state. Crystalline solids of DMMF gives excimer like emission with emission maximum at 550 nm. DMMF displays photodecomposition in chloromethane solvents by electron transfer from the excited DMMF molecule to the solvent molecule. DFT/TD-DFT methods were used to study the geometric and electronic structures of DMMF in different solvents. A noticeable good agreement was found between the experimental and theoretical results.

References

1. Denes F, Pichowicz M, Povie G, Renaud P (2014) Thiyl radicals in organic synthesis. Chem Rev 114:2587–2693
2. Kovacic P, Jones MB (1987) Dehydro coupling of aromatic nuclei by catalyst-oxidant systems: poly(p-phenylene). Chem Rev 87: 357–379
3. Yoshizawa M, Klosterman JK (2014) Molecular architectures of multi-anthracene assemblies. Chem Soc Rev 43:1885–1898
4. Wang C, Dong H, Hu W, Liu Y, Zhu D-B (2012) Semiconducting π-conjugated systems in field-effect transistors: a material Odyssey of organic electronics. Chem Rev 112:2208–2267
5. Arias AC, MacKenzie JD, McCulloch I, Rivnay J, Salleo A (2010) Materials and applications for large area electronics: solution-based approaches. Chem Rev 110:3–24
6. Clarke TM, Durrant JR (2010) Charge photogeneration in organic solar cells. Chem Rev 110:6736–6767
7. Watson M, Fechtenkotter A, Mullen K (2001) Big is beautiful –"aromaticity" revisited from the viewpoint of macromolecular and supramolecular benzene chemistry. Chem Rev 101:1267–1300
8. Figueira-Duarte TM, Mullen K (2011) Pyrene-based materials for organic electronics. Chem Rev 111:7260–7314
9. Ahmed SA (2009) Photochromism of dihydroindolizines. Part 12: synthesis and photochromism of novel π-conjugated rigid dihydroindolizines as potential molecular electronic devices. Tetrahedron 65:1373–1388
10. Ahmed SA, Hozien ZA, Abdel-Wahab AA, Al-Raqa SY, Al-Simaree AA, Mousa Z, Al-Amri SN, Messali M, Soliman SA, Dürr H (2011) Photochromism of dihydroindolizines. Part 16: tuning of the photophysical behavior of photochromic dihydroindolizines in solution and in polymeric thin film. Tetrahedron 67:7173–7184
11. Ahmed SA, Al-Raqa SY (2011) Photochromism of dihydroindolizines: part XIV. Synthesis and photophysical behavior of photochromic dihydroindolizine-tripodal linkers toward anchoring sensitizers to semiconductor nanoparticles. J Phys Org Chem 24:173–184
12. Hu J-Y, Yamato T (2011) Organic light emitting diode—material. In: Ko S-H (ed) Process and devices. InTech, Croatia, pp 21–60
13. Yang SW, Elangovan A, Hwang KC, Ho TI (2005) Electronic polarization reversal and excited state intramolecular charge transfer in donor/acceptor ethynylpyrenes. J Phys Chem B 109:16628–16635
14. Ni X-L, Wang S, Zeng X, Tao Z, Yamato T (2011) Pyrene-linked triazole-modified Homooxacalix[3]arene: a unique C3symmetry ratiometric fluorescent chemosensor for Pb2+. Org Lett 13:552–555
15. Omer KM, Ku S-Y, Wong K-T, Bard AJ (2009) Efficient and stable blue electrogenerated chemiluminescence of fluorene-substituted aromatic hydrocarbons. Angew Chem Int Ed 48:9300–9303
16. Tao S, Peng Z, Zhang X, Wang P, Lee C-S, Lee S-T (2005) Highly efficient non-doped blue organic light-emitting diodes based on fluorene derivatives with high thermal stability. Adv Funct Mater 15:1716–1721
17. Huang L, Wu SP, Qu Y, Geng YH, Wang FS (2008) Grignard metathesis chain-growth polymerization for polyfluorenes. Macromolecules 41:8944–8947

18. Hong Y, Lam JWY, Tang BZ (2011) Aggregation-induced emission. Chem Soc Rev 40:5361–5388
19. Hatchard IG, Parker CA (1956) A new sensitive chemical actinometer. II. potassium ferrioxalate as a standard chemical actinometer. Proc Roy Soc London A235:518–536
20. El-Daly SA, Hazmy SM, Ebeid EM, Bhasikuttan AC, Palit DK, Spare AV, Mittal JP (1996) Spectral, acid−base, and laser characteristics of 1,4-Bis[β-(2-quinolyl)vinyl]benzene (BQVB). J Phys Chem 100:9732–9737
21. Lakowicz JR (2006) Principles of fluorescence spectroscopy, 3rd edn. Springer, New York
22. Dutta A, Dutta RK (2014) Fluorescence behavior of cis-methyl orange stabilized in cationic premicelles. Spectrochim Acta A Mol Biomol Spectrosc 126:270–279
23. Sierocki P, Maas H, Dragut P, Richardt G, Vogtle F, Cola LD, Brouwer FAM, Zink JI (2006) Photoisomerization of azobenzene derivatives in nanostructured silica. J Phys Chem B 110:24390–24398
24. Sakamoto R, Kume S, Sugimoto M, Nishihara H (2009) Trans–cis photoisomerization of azobenzene-conjugated dithiolato-bipyridine platinum(II) complexes: extension of photoresponse to longer wavelengths and photocontrollable tristability. Chem Eur J 15:1429–1439
25. Zhuang X, Ha T, Kim HD, Centner T, Labeit S, Chu S (2000) Fluorescence quenching: a tool for single-molecule protein-folding study. Proc Natl Acad Sci U S A. 97:14241–14244
26. Kim DY, Cho HN, Kim CY (2000) Blue light emitting polymers. Prog Polym Sci 25:1089–1139
27. Lippert E (1957) Spektroskopische Bestimmung des Dipolmomentes aromatischer Verbindungen im ersten angeregten Singulettzustand. Z Elektrochem 61:962–975
28. Suppan P (1990) Invited review solvatochromic shifts: the influence of the medium on the energy of electronic states. J Photochem Photobiol A Chem 50:293–330
29. Lakowicz JR (2006) Principles of fluorescence spectroscopy, 3rd edn. Springer, New York, p 209 (Chapter 6)
30. Biondic MC, Erra-Balsells R (1994) Photochemical reaction of full-aromatic β-carbolines in halomethanes 2. CHCl3: electronic spectra and kinetics. Photochem Photobiol A Chem 77:149–159
31. Biondic MC, Erra-Balsells R (1990) Photochemical reaction of β-carbolines in carbon tetrachloride-ethanol mixtures. Photochem Photobiol A Chem 51:341–353
32. Mastsuda MCS, Kokado R, Inou HE (1970) The photoconductivity in a CCl4 solution of N,N-dimethylaniline. Bull Chem Soc Jpn 43: 2994–2995
33. Balsells RE, Farsca AR (1988) Photochemical reactions of aliphatic-amines in dichloromethane solution. Aust J Chem 41: 103–110
34. Wolinski L, Turznski Z, Witkowski K (1987) Lichtstreubefunde zur Kettenspaltung von Polystyrol in sauerstoffreien CCl4- und CHCl3-Lösungen bei Lichteinwirkung der Wellenlängen $\lambda \geq 270$ nm. Macromol Chem Phys 188:2895–2907
35. Bard AJ, Ledwith A, Shine HJ (1976) Formation, properties and reactions of cation radicals in solution. Adv Phys Org Chem 13: 155–278
36. El-Daly SA, Fayed TA (2000) Photochemistry of N, Ń-ditridecyl-3, 4:9,10-perylenetetracarboxylic diimide in chloromethane solvents. J Photochem Photobiol A Chem 137:15–19
37. El-Daly SA, Asiri AM, Alamry K, Khan SA (2013) Spectroscopic studies and laser activity of 3-(4-dimethylamino-phenyl)-1-(2,5-dimethyl-furan-3-yl)-propenone (DDFP): a new green laser dye. J Lumin 137:6–14
38. Frisch MJ, Trucks GW, Schlegel HB, Scuseria GE, Robb MA, Cheeseman JR, Scalmani G, Barone V, Mennucci B, Petersson GA, Nakatsuji H, Caricato M, Li X, Hratchian HP, Izmaylov AF, Bloino J, Zheng G, Sonnenberg JL, Hada M, Ehara M, Toyota K, Fukuda R, Hasegawa J, Ishida M, Nakajima T, Honda Y, Kitao O, Nakai H, Vreven T, Montgomery JA Jr, Peralta JE, Ogliaro F, Bearpark M, Heyd JJ, Brothers E, Kudin KN, Staroverov VN, Kobayashi R, Normand J, Raghavachari K, Rendell A, Burant JC, Iyengar SS, Tomasi J, Cossi M, Rega N, Millam JM, Klene M, Knox JE, Cross JB, Bakken V, Adamo C, Jaramillo J, Gomperts R, Stratmann RE, Yazyev O, Austin AJ, Cammi R, Pomelli C, Ochterski JW, Martin RL, Morokuma K, Zakrzewski VG, Voth GA, Salvador P, Dannenberg JJ, Dapprich S, Daniels AD, Farkas O, Foresman JB, Ortiz JV, Cioslowski J, Fox DJ (2009) Gaussian 09, Revision A.02. Gaussian, Inc, Wallingford
39. Frisch A, Dennington RD II, Keith TA, Milliam J, Nielsen AB, Holder AJ, Hiscocks J (2007) GaussView Reference, Version 5.0. Gaussian Inc, Pittsburgh
40. Wolinski JK, Hincon JF, Pulay P (1990) Efficient implementation of the gauge-independent atomic orbital method for NMR chemical shift calculations. J Am Chem Soc 112:8251–8260
41. Gross EKU, Kohn W (1990) Time-dependent density-functional theory. Adv Quant Chem 21:255–291
42. Cances E, Mennucci B, Tomasi J (1997) A new integral equation formalism for the polarizable continuum model: theoretical background and applications to isotropic and anisotropic dielectrics. J Chem Phys 107:3032–3041
43. Lide DR Jr, Mann DE (1958) Microwave spectra of molecules exhibiting internal rotation. III. trimethylamine. J Chem Phys 28: 572–576
44. Gerkin RE, Lundstedt AP, Reppart WJ (1984) Structure of fluorene, C13H10, at 159 K. Acta Crystallogr C40:1892–1894
45. Alecu IM, Zheng J, Zhao Y, Truhlar DG (2010) Computational thermochemistry: scale factor databases and scale factors for vibrational frequencies obtained from electronic model chemistries. J Chem Theory Comput 6:2872–2887
46. Silverstein RM, Bassler GC, Morrill TC (1991) Spectrometric identification of organic compounds. John Willey, Chistester
47. Karabacak M, Cinar M (2012) FT-IR, FT-Raman, UV spectra and DFT calculations on monomeric and dimeric structure of 2-amino-5-bromobenzoic acid. Spectrochim Acta A 86:590–599
48. Chattaraj PK, Maiti B (2003) HSAB principle applied to the time evolution of chemical reactions. J Am Chem Soc 125:2705–2710
49. Pearson RG (2005) Chemical hardness and density functional theory. J Chem Sci 117:369–377
50. Aurell MJ, Domingo LR, Perez P, Contreras R (2004) A theoretical study on the regioselectivity of 1,3-dipolar cycloadditions using DFT-based reactivity indexes. Tetrahedron 60:11503–11509
51. Reed EA, Curtiss LA, Weinhold F (1988) Intermolecular interactions from a natural bond orbital, donor-acceptor viewpoint. Chem Rev 88(6):899–9026
52. Reed EA, Weinhold F (1983) Natural bond orbital analysis of near-Hartree–Fock water dimer. J Chem Phys 78(6):4066–4073
53. Song L, Lin Y, Wu W, Zhang Q, Mo Y (2005) Steric strain versus hyperconjugative stabilization in ethane congeners. J Phys Chem A 109(10):2310–2316